Night-time Ventilation Experiments

Artmann, Nikolai; Jensen, Rasmus Lund

Publication date:
2008

Document Version
Publisher's PDF, also known as Version of record

Night-time ventilation experiments

Setup, data evaluation and uncertainty assessment

N. Artmann
R. L. Jensen

ISSN 1901-726X
DCE Technical Report No. 053

AALBORG UNIVERSITY
Department of Civil Engineering

Aalborg University
Department of Civil Engineering
Indoor Environmental Engineering Research Group

DCE Technical Report No. 053

Night-time ventilation experiments

Setup, data evaluation and uncertainty assessment

by

N. Artmann
R. L. Jensen

October 2008

Scientific Publications at the Department of Civil Engineering

Technical Reports are published for timely dissemination of research results and scientific work carried out at the Department of Civil Engineering (DCE) at Aalborg University. This medium allows publication of more detailed explanations and results than typically allowed in scientific journals.

Technical Memoranda are produced to enable the preliminary dissemination of scientific work by the personnel of the DCE where such release is deemed to be appropriate. Documents of this kind may be incomplete or temporary versions of papers—or part of continuing work. This should be kept in mind when references are given to publications of this kind.

Contract Reports are produced to report scientific work carried out under contract. Publications of this kind contain confidential matter and are reserved for the sponsors and the DCE. Therefore, Contract Reports are generally not available for public circulation.

Lecture Notes contain material produced by the lecturers at the DCE for educational purposes. This may be scientific notes, lecture books, example problems or manuals for laboratory work, or computer programs developed at the DCE.

Theses are monograms or collections of papers published to report the scientific work carried out at the DCE to obtain a degree as either PhD or Doctor of Technology. The thesis is publicly available after the defence of the degree.

Latest News is published to enable rapid communication of information about scientific work carried out at the DCE. This includes the status of research projects, developments in the laboratories, information about collaborative work and recent research results.

Published 2008 by
Aalborg University
Department of Civil Engineering
Sohngaardsholmsvej 57,
DK-9000 Aalborg, Denmark

Printed in Aalborg at Aalborg University

ISSN 1901-726X
DCE Technical Report No. 053

Table of contents

Setup of the test room

Originally, 'DET LILLE HUS PÅ PRÆRIEN' (Figure 1 to Figure 3) was a wooden construction insulated with 100 mm rock wool. The internal surfaces were covered with 19 mm plywood. Externally the walls were covered with 16 mm wooden boards and the roof with 22 mm plywood. In previous experiments the chamber was used to simulate a room with an external facade. Therefore a small part was separated to simulate the outdoor climate. The separation wall was insulated with 240 mm rock wool and covered with 12 mm chipboards on both sides.

For a previous PhD study on night time ventilation by Jensen [1] a massive ceiling element made of 7 layers of 12.5 mm gypsum boards was installed. For additional insulation, a layer of 50 mm rock wool between wooden beams was placed between the ceiling element and the former roof. In total 110 thermocouples were installed in 5 different layers of the ceiling element.

For the experiments described here, additional insulation was installed at the internal surfaces in order to improve the boundary conditions. The insulation was installed in 3 layers, so that sensors could be placed in-between. The total thickness of the insulation made of expanded polystyrene (EPS) was 160 mm (30 + 30 + 100) at the walls and 230 mm (100 + 30 + 100) at the floor. Along the edge of the ceiling the gypsum boards were cut, so that the new insulation could be extended to the rock wool layer (Figure 3).

After installation of the insulation the internal dimensions were 2.64 m x 3.17 m x 2.93 m (width x length x height) resulting in a volume of 24.52 m^3.

Figure 1. The test room 'DET LILLE HUS PÅ PRÆRIEN'

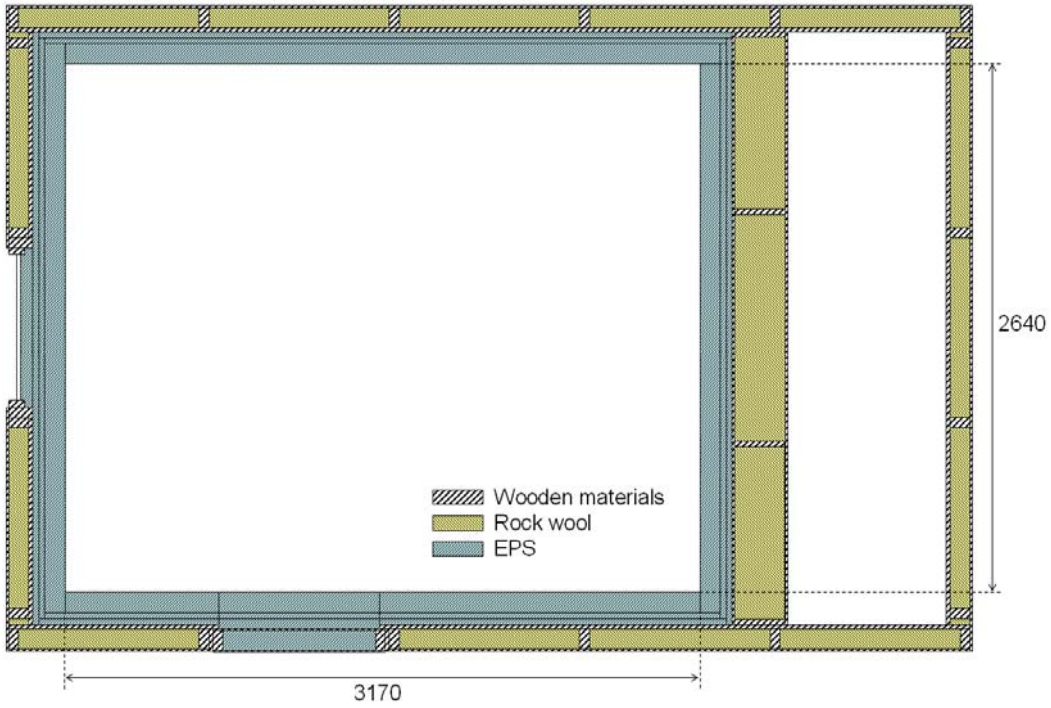

Figure 2. Plan view of the test room.

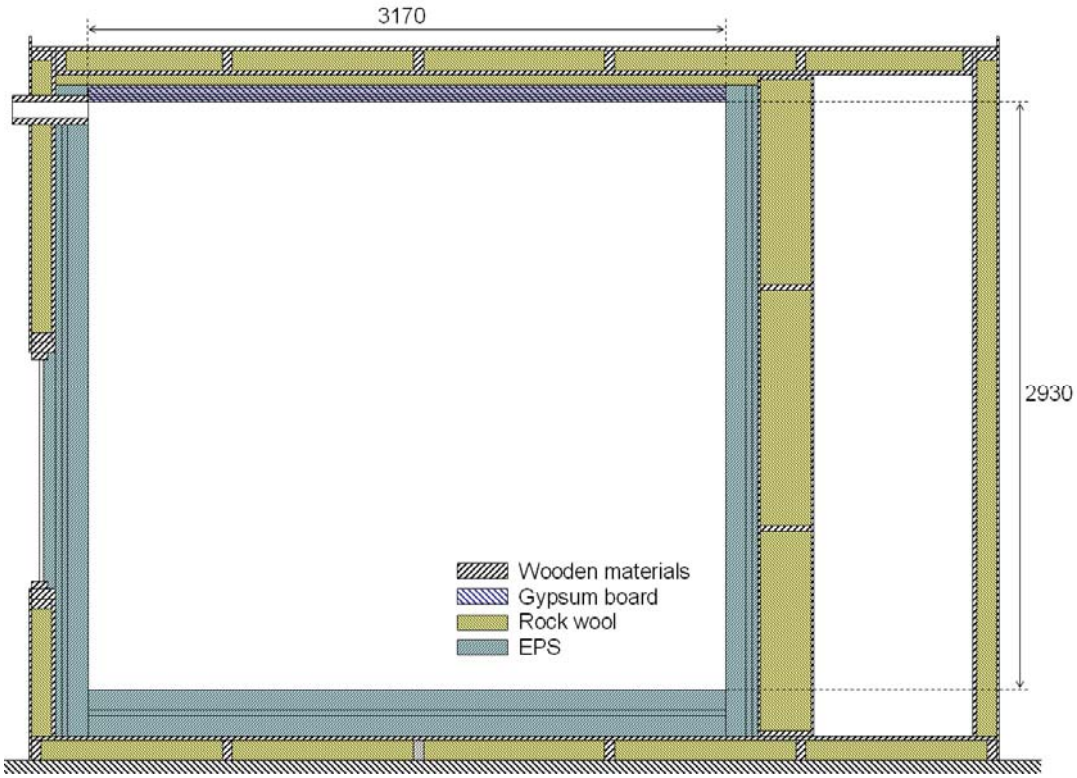

Figure 3. Vertical section of the test room

Ventilation system

A mechanical ventilation system was installed to supply air at a defined temperature to the test room. A schematic diagram of the ventilation system is shown in Figure 4. Air is taken from the lab and flows through

a filter and two heat exchangers for cooling and heating. The heating and cooling power is controlled by motor-operated valves and a PID controller. The temperature sensor for the controller is placed after the fan. The fan speed can be controlled by a frequency transformer to set the air flow rate. The ventilation system was capable of providing an air flow rate of about 56 - 330 m^3/h, corresponding to 2.3 - 13 air changes per hour (ACH).

In order to obtain stable supply air conditions at the beginning of an experiment, a bypass valve was installed. By switching the bypass valve, ventilation of the test room can be started without changing the air flow rate through the air conditioning unit. In order to achieve the same flow rate through the bypass and the test room, the resistance of the bypass was adjusted by a control valve at the end of the bypass. Orifices for measuring the flow rate were installed in the supply air pipe to the test room and in the bypass. The pressure difference over the orifice was measured using a micro-manometer. Two different orifices with 100 mm and 160 mm diameter were used for low and high airflow rates, respectively. The accuracy of the air flow measurement was about ± 5 %.

Another fan with variable speed was installed in the exhaust pipe. To prevent air from flowing through leakages into the test room, the speed of the exhaust fan was adjusted aiming a very small overpressure (0.1 Pa) in the test room.

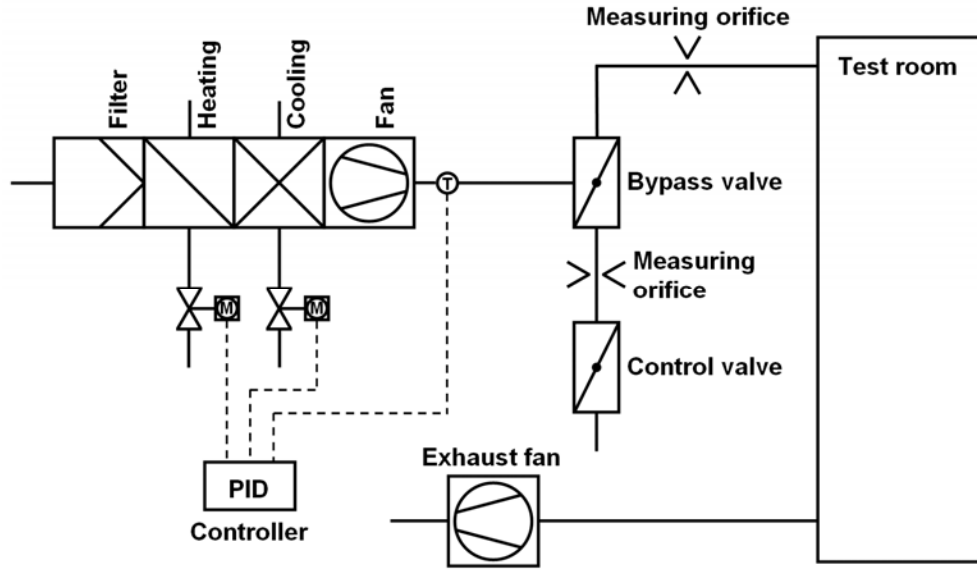

Figure 4. Schematic diagram of the ventilation system.

Two different configurations of the air in- and outlet openings of the test room representing mixing and displacement ventilation were investigated (Figure 5). In case of mixing ventilation, the air inlet to the test room was a rectangular opening of 830 mm width and 80 mm height located directly below the ceiling (Figure 6). To obtain a uniform velocity profile, two fleece filters were placed approximately 25 and 35 cm before the opening. For the air outlet there were two circular openings of 110 mm close to the floor.

For displacement ventilation the same rectangular opening below the ceiling was used as outlet and a semicircular displacement inlet device was placed at the floor on the same side of the test room (Figure 7).

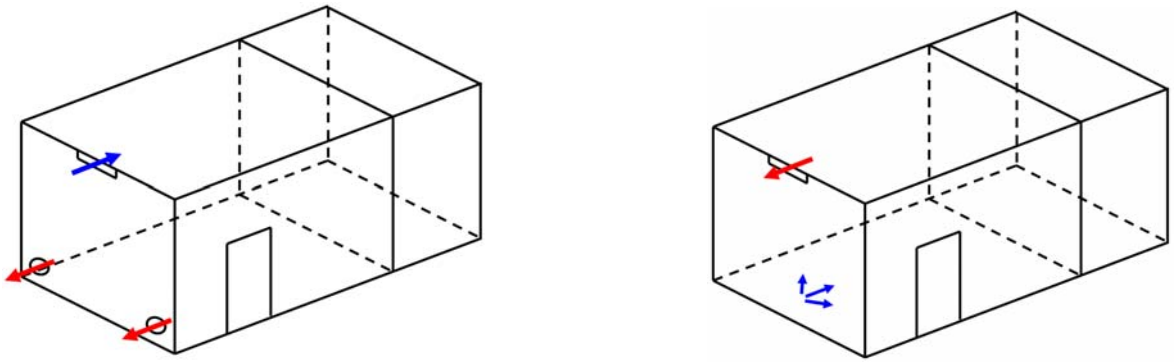

Figure 5. Configurations of the air in- and outlet openings of the test room for mixing (left) and displacement (right) ventilation

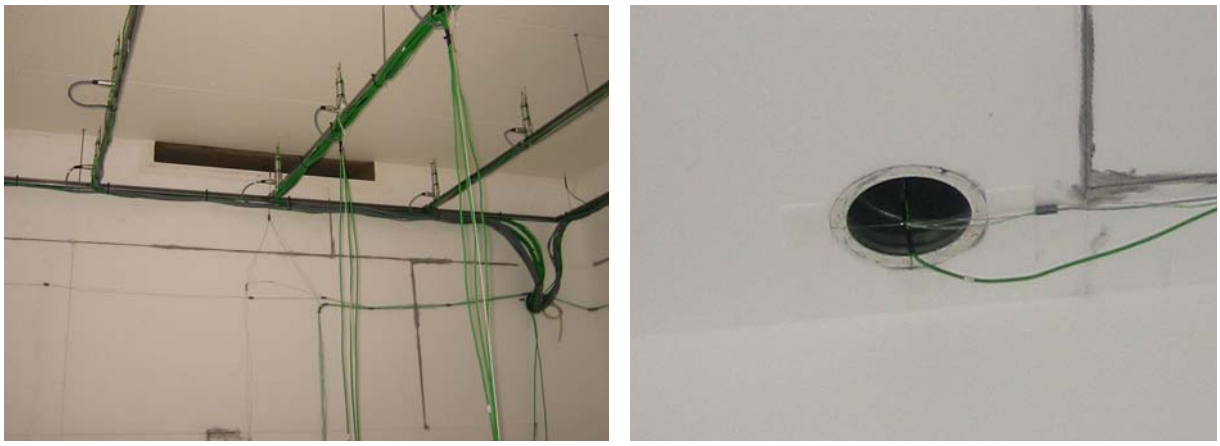

Figure 6. Ventilation openings. Left: Opening used as air inlet for mixing ventilation and outlet for displacement ventilation. Right: Outlet opening for mixing ventilation.

Figure 7. Inlet device for displacement ventilation.

Material properties

The thermal properties of the materials used at the internal surfaces of the test room are important for the data evaluation. The thermal conductivity, λ, the specific heat capacity, c and the density, ρ of the gypsum boards (Gyproc Gulvplank) used for the ceiling element were measured at Empa (Swiss federal laboratories

for materials testing and research). The thermal conductivity, λ and the density, ρ of the EPS (Sundolitt S80) used at the walls and the floor were also measured at Empa. For the specific heat capacity, *c* of the EPS the value given in the European standard EN 12524 [2] was used.

For the calculation of the radiative heat flows between the internal surfaces the emissivities need to be known. The ceiling was painted with white paint. The emissivity, ε of a sample painted with the same paint was measured at Empa using a calorimetric method. Because of the low thermal conductivity and the partial transparency the calorimetric method did not work for EPS. Therefore the emissivity of EPS was measured at ZAE Bayern using a Fourier-Transformation-InfraRed (FTIR) spectrometer and an integrating sphere [3].

The material properties including uncertainties are summarised in Table 1.

For the determination of the air flow rate the density of the air was calculated according to the temperature and the humidity in the lab and the atmospheric pressure. The heat capacity of the air was assumed to be constant, c_{Air} = 1005 J/kgK.

Table 1. Properties of the materials used at the internal surfaces of the test room.

	λ (W/mK)	ρ (kg/m^3)	c (J/kgK)	ε (-)
Gypsum board	0.28 ± 0.01	1127 ± 10	1006 ± 100	-
Expanded polysteren (EPS)	0.037 ± 0.001	16.0 ± 0.1	1450 ± 100	0.73 ± 5%
White paint (Ceiling)	-	-	-	0.90 ± 5%

Measurement instrumentation and location of sensors

For temperature measurements two Fluke Helios Plus 2287A data loggers with 100 channels each and one Grant Squirrel 2040 data logger with 32 channels were used. The setup of the Helios data loggers using 178 channels for temperature measurement and 17 channels for temperature difference measurement is described in detail in [4]. The accuracy of the measurement system using the Helios data loggers was estimated to be ± 0.086 K [4]. The accuracy of the Grant Squirrel 2040 for temperature measurements using type K thermocouples is given as ± 1.4 K [5]. All thermocouples needed for the data evaluation were connected to the more accurate Helios system (sensor configuration see Table A1). The Squirrel data logger was used to monitor the inlet air temperature, and the boundary conditions (sensor configuration see Table A2). The Helios and the Squirrel data loggers were configured to record temperatures at a sampling rate of 0.1 Hz.

For air flow velocity measurements a Dantec 54N10 Multichannel Flow Analyzer with 18 hot sphere anemometers was used. The anemometers were calibrated for horizontal flow in the range from 0 to 1 m/s. Velocity measurements were integrated over 120 s with 30 s pause between integration periods.

The ceiling was divided into 22 sections (Figure 8). Originally the sensors were placed in the centre of each section. Although this symmetry was broken after cutting the gypsum boards and installing the EPS, the size of the sections was still determined as shown in Figure 8. At each of the 22 positions 5 thermocouples were installed in different layers, totalling 110 thermocouples. Additional thermocouples were installed 30 mm below the ceiling to measure the local air temperature (Figure 9).

The anemometers were installed 30 mm below the ceiling at the same positions as the temperature sensors. As only 18 anemometers were available, no velocity sensors were installed at positions 1, 5, 6 and 10

(Figure 8). In order not to disturb the air flow measurements, the thermocouples for the air temperature measurement were installed in the back of the anemometers (Figure 10).

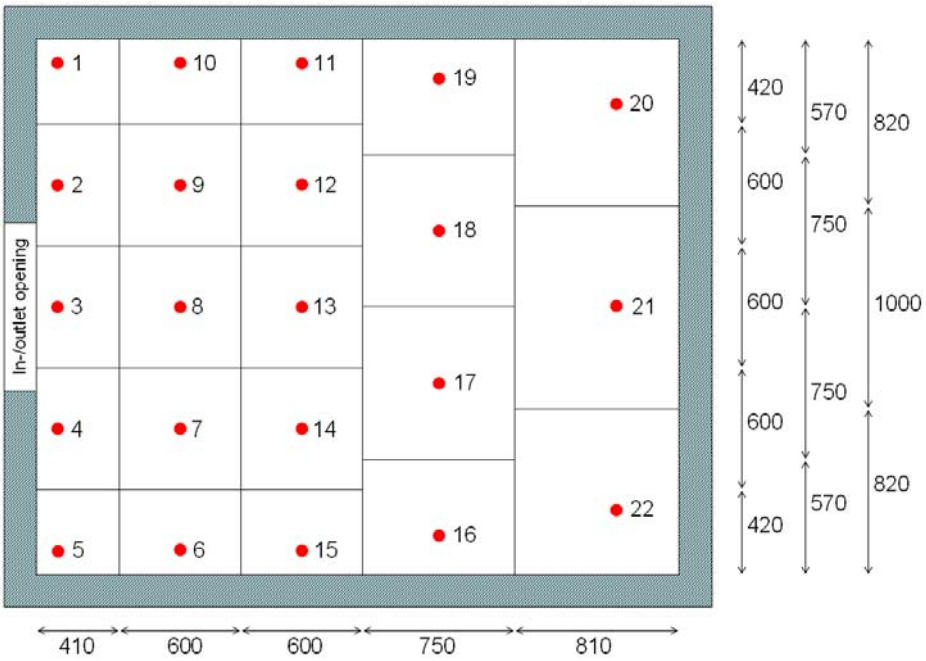

Figure 8. Subdivision of the ceiling into 22 sections and location of sensors (top view).

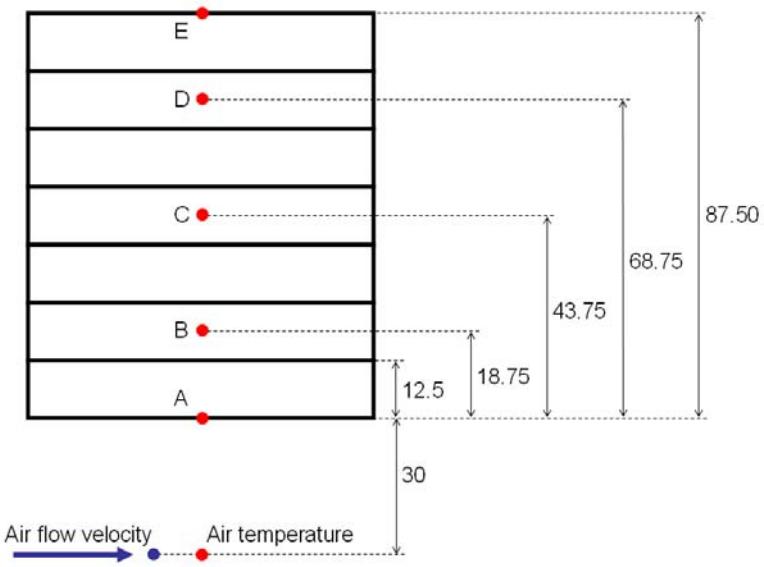

Figure 9. Vertical section of the ceiling element indicating the location of thermocouples for measuring the temperature in different layers (A - E) and the local air temperature; anemometer for air flow velocity measurement.

Figure 10. Anemometer and thermocouples for local air and ceiling surface temperature measurement.

The walls and the floor were divided into 3 sections each, and sensors were located in the centre of each section (Figure 11). At each position one thermocouple connected to the Squirrel data logger was installed at the internal surface of the plywood board. Then the first layer of insulation (walls: 30 mm, floor: 100 mm) was installed. The temperature difference over the second layer of EPS (30 mm) was measured with thermopiles made of 4 thermocouples (Figure 13, left). The temperature difference was used to calculate the heat flow through the walls and the floor. At all positions indicated in Figure 11 additional thermocouples were installed to measure the internal surface and the local air temperature at a distance of 30 mm from the surface (Figure 13, right).

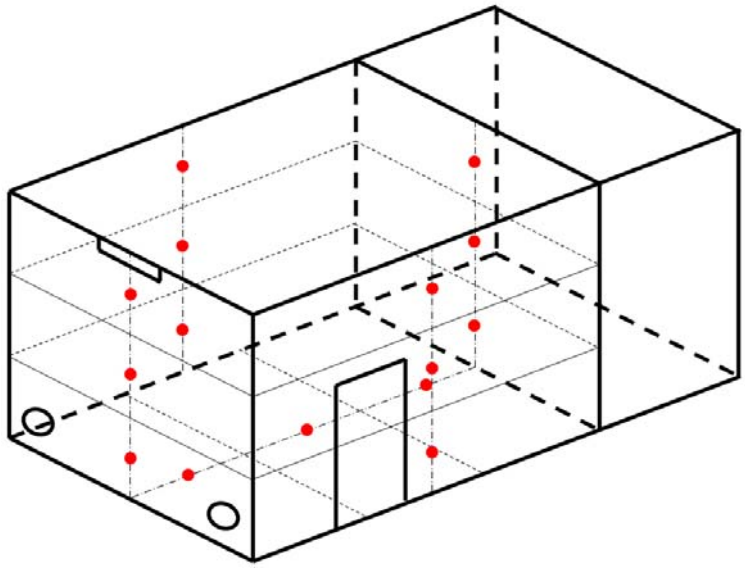

Figure 11. Subdivision of the walls and the floor into 3 sections and location of sensors.

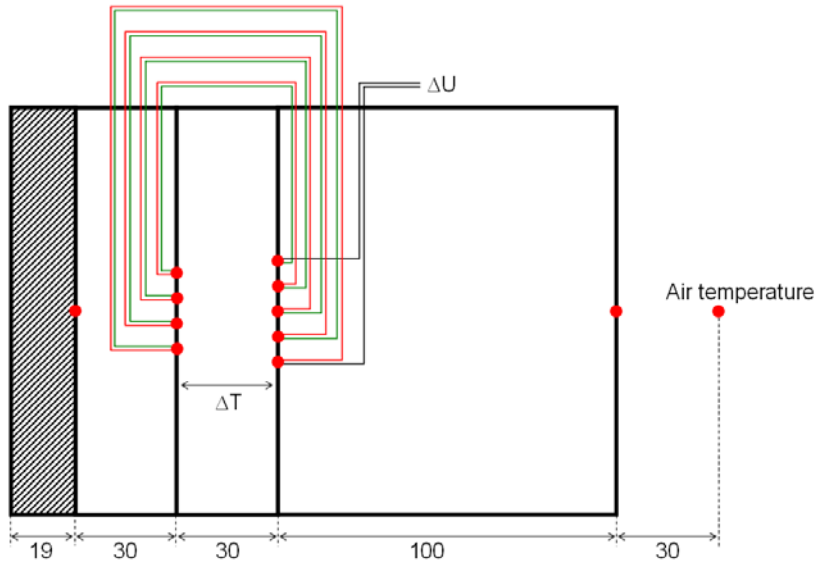

Figure 12. Location of thermocouples in different layers of the walls; thermopile for temperature difference (heat flow) measurement.

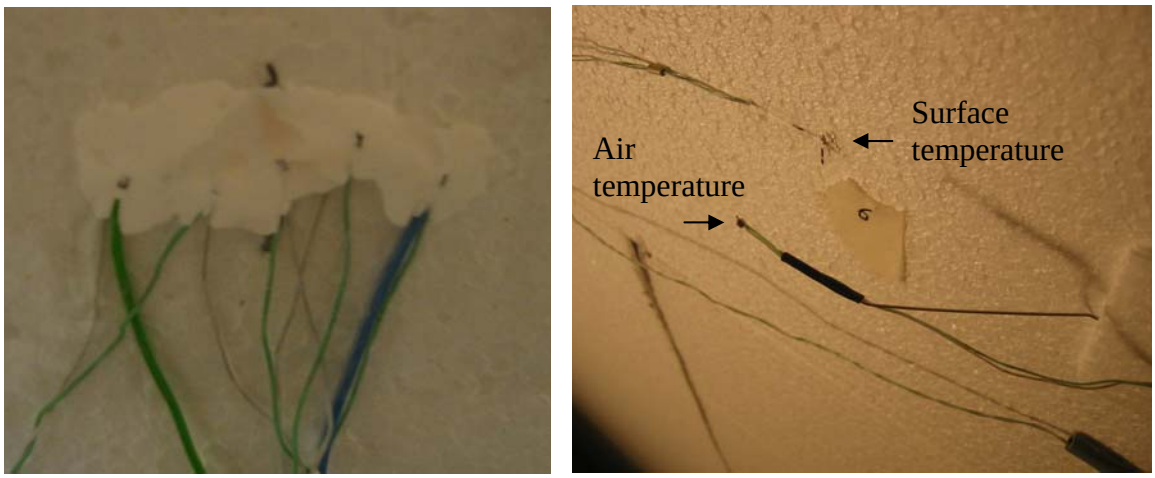

Figure 13. Internal junctions of the thermopile used for temperature difference measurement (left). Thermocouples for wall surface and local air temperature measurements (right).

To measure the air temperature distribution in the room 3 columns of thermocouples were installed in the vertical central plane. The columns were located below the 2nd, 3rd and 4th row of sensors at the ceiling, i.e. positions 8, 13, and between 17 and 18 (Figure 8). In these columns thermocouples were at heights 0.1, 1.1, 1.7, 2.6 and 2.9 m above the floor (Figure 14). The height 2.9 m above the floor is equal to 30 mm below the ceiling (sensors for local air temperature at the ceiling).

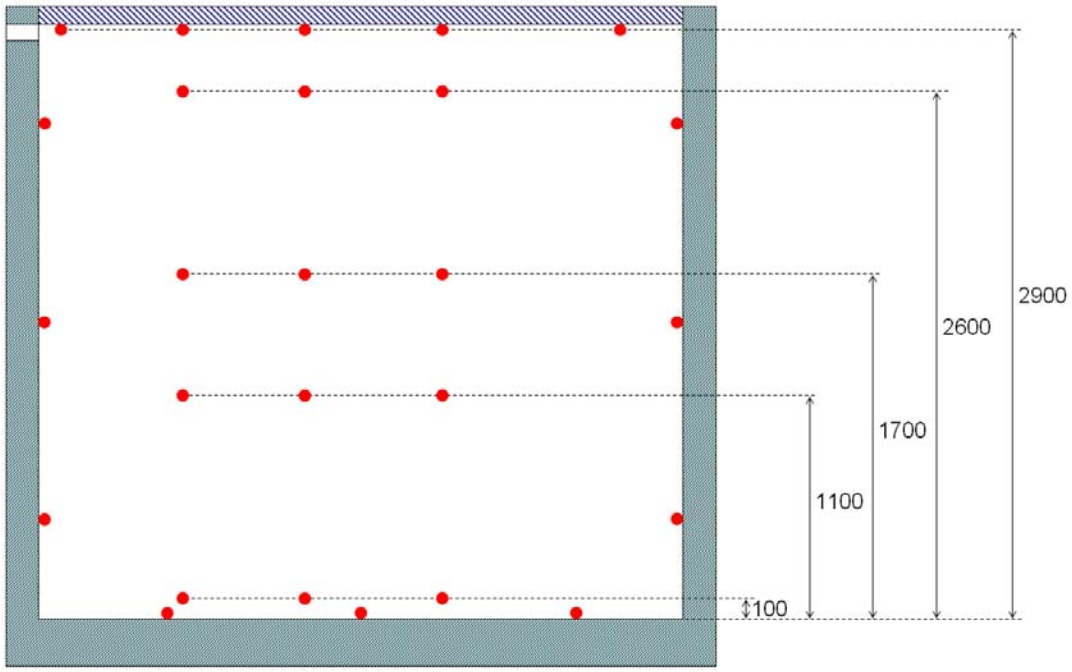

Figure 14. Thermocouples for air temperature measurements in the vertical central plane

For determination of the total heat flow removed from the test room by ventilation, the inlet and outlet air temperatures were measured. In case of mixing ventilation, sensors were placed in the centre of the inlet and both outlet openings (Figure 15). For higher accuracy, additionally, the temperature differences between the in- and outlet openings were measured using thermopiles made of 2 thermocouples. In case of displacement ventilation the sensors for the inlet air temperature measurement were installed where the pipe enters the room and in the inlet device (Figure 7). The outlet air temperature was measured using the same sensor as for the inlet during mixing ventilation (Figure 15, left).

Figure 15. Thermocouples for measuring inlet (left) and outlet (right) temperatures during mixing ventilation.

Procedure for experiments

In each experiment the response of the test room to a step in the air flow rate (inflow temperature below room temperature) was measured for at least 12 hours. In total 16 experiments with different ventilation modes, air change rates (*ACR*) and initial temperature differences (ΔT_0) were conducted (Table 2). The

experiments were started with the test room having a homogeneous temperature equal to the lab temperature. In order to obtain stable supply air conditions and a homogeneous temperature in the test room at the beginning of the experiment, the settings of the ventilation system (supply fan, exhaust fan, inflow set point, chiller set point) were adjusted about 36 hours before the experiment was started. During these 36 hours the air was piped through the bypass. The experiment was then started by switching the bypass valve to the test room. Because of the thermal mass of the pipe between the bypass valve and the test room, it still took some time until the temperature measured at the inlet was constant (cf. Figure 16). The initial temperature difference, ΔT_0 was therefore defined as the difference between the mean temperature of the ceiling element and the mean inlet air temperature measured during the last 10 hours of the experiment.

Table 2. List of experiments.

No	Ventilation mode	ACR (ACH)	ΔT_0 (K)	File No
1	Mixing ventilation	2.3	7.9	016
2	Mixing ventilation	3.3	4.3	014
3	Mixing ventilation	3.3	10.2	015
4	Mixing ventilation	6.7	2.9	010
5	Mixing ventilation	6.8	6.1	008
6	Mixing ventilation	6.6	8.9	006
7	Mixing ventilation	13.1	2.9	011
8	Mixing ventilation	13.2	4.0	009
9	Mixing ventilation	13.1	5.3	007
10	Mixing ventilation	13.3	9.2	002
11	Displacement ventilation	3.1	10.1	017
12	Displacement ventilation	6.7	5.8	019
13	Displacement ventilation	6.7	11.3	018
14	Displacement ventilation	12.6	3.6	022
15	Displacement ventilation	12.6	6.0	021
16	Displacement ventilation	12.7	12.7	020

Data evaluation

For the evaluation of the heat transfer at the internal room surfaces, first the total surface heat flow (conduction in the material) for each section was calculated from the measured temperatures. Also the radiative heat flow between the surfaces was calculated from the measured surface temperatures. The difference between conduction and radiation then yielded the convective heat flow.

By way of example, Figure 16 shows the measured temperatures of the inlet air and for position 8, the local air and 5 different layers of the ceiling. For the calculation of the conduction, the temperatures measured at the internal and external surface were used as boundary condition for a transient 1-dimensional finite difference model using an explicit scheme. To reduce the noise in the measurement signals the moving average of 15 values (2.5 minutes) was applied. Running the model resulted in the spatial temperature profile for each time step. For each section, *i* the conductive heat flux, $\dot{q}_{cond,i}$ at the surface was calculated from the temperature gradient.

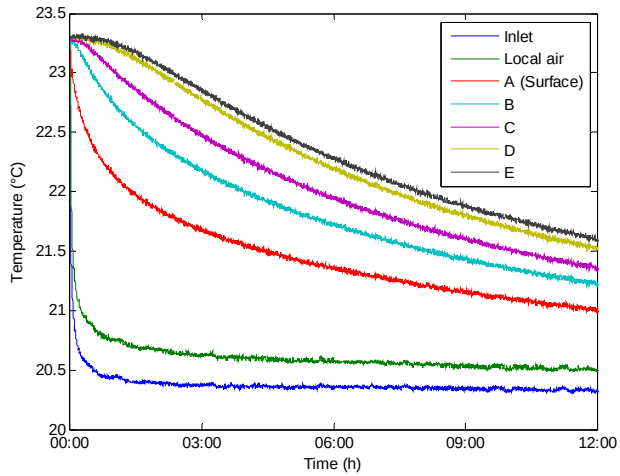

Figure 16. Temperatures measured at position 8 during experiment no. 4 with mixing ventilation with 6.7 ACH and an initial temperature difference of ΔT_0 = 2.9 K (A-E: 5 different layers of the ceiling).

The heat flows through the walls and the floor were calculated from the measured temperature difference over a 30 mm layer of EPS. In order to account for the thermal mass of the EPS, the heat flow at the internal wall and floor surfaces was calculated using the same method as at the ceiling. Here the internal surface temperature and the external heat flow were used as boundary condition for the finite difference model.

For calculation of the radiative heat flows, the view factors $F_{i,j}$ between all 22 sections of the ceiling and 3 sections of each wall and the floor were determined according to [6]. The radiative heat flux $\dot{q}_{rad\,i}$ from the surface A_i was obtained as sum of the heat fluxes to all surfaces A_j applying the measured surface temperatures:

$$\dot{q}_{rad,i} = \sum_j \frac{\sigma \cdot \varepsilon_i \cdot \varepsilon_j \cdot F_{i,j}}{1-(1-\varepsilon_i)(1-\varepsilon_j)\cdot F_{i,j}\cdot F_{i,j}} \left(T_i^{\,4} - T_j^{\,4}\right)$$

Where $\sigma = 5.67 \cdot 10^{-8}\, W/\left(m^2 K^4\right)$ is the Stefan-Boltzmann constant, and ε_i and ε_j are the emissivities of the surfaces.

The convective heat flux, $\dot{q}_{conv,\,i}$ for each section, *i* was then obtained from the difference between the conductive and radiative heat fluxes. Figure 17 shows the convective heat flux for different sections of the ceiling. The conductive, radiative and convective heat fluxes were integrated over all 22 sections of the ceiling to obtain the total heat flows at the ceiling surface. The total conductive, radiative and convective heat flows at the ceiling surface are displayed in Figure 18.

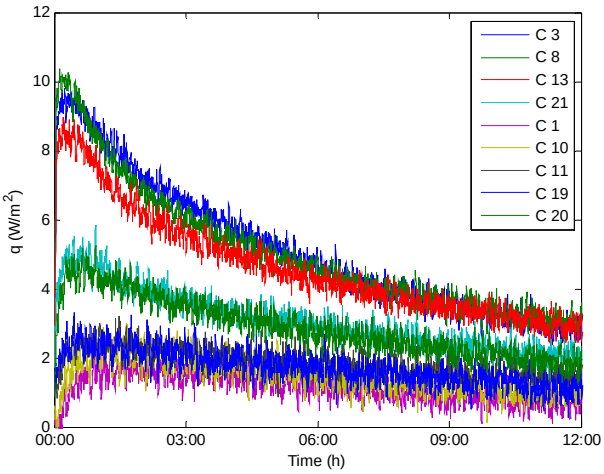

Figure 17. Convective heat flux for different sections of the ceiling during experiment no. 4 with mixing ventilation with 6.7 ACH and an initial temperature difference of ΔT_0 = 2.9 K.

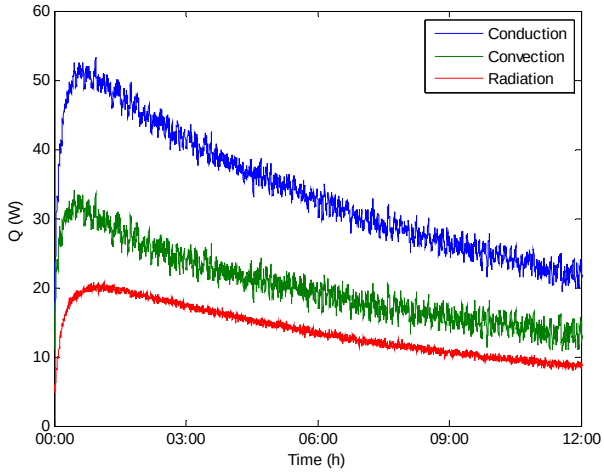

Figure 18. Total conductive, convective and radiative heat flows at the ceiling surface during experiment no. 4 with mixing ventilation with 6.7 ACH and an initial temperature difference of ΔT_0 = 2.9 K.

Integrating the convective heat flux over all room surfaces results in the total heat flow removed from the test room, $\dot{Q}_{conv,tot}$:

$$\dot{Q}_{conv,tot} = \sum_i A_i \cdot \dot{q}_{conv,i}$$

It should be noted, that the total convective heat flow, $\dot{Q}_{conv,tot}$ equals the total conductive heat flow, $\dot{Q}_{cond,tot}$, as by radiation heat is only transported from one surface to another ($\dot{Q}_{rad,tot} = 0$).

Alternatively, the total heat flow removed from the room can also be determined from the air flow rate, $\dot{V}_{Air}$, the density, ρ_{Air} , the heat capacity, $c_{p,Air}$ and the temperature difference between the in- and outflowing air.

$$\dot{Q}_{vent,tot} = \dot{V}_{Air} \cdot \rho_{Air} \cdot c_{p,Air} \cdot (T_{Outlet} - T_{Inlet})$$

Figure 19 compares the total heat flow obtained by the two different methods. The difference visible at the beginning of the experiment results from the thermal capacity of the air in the room. In the experiment shown in Figure 19, left the two methods are in very good agreement. In other cases a difference up to 18 % was found due to measurement uncertainties (Figure 19, right). It stands out, that in all experiments with mixing ventilation $\dot{Q}_{vent,\,tot}$ is larger than $\dot{Q}_{conv,\,tot}$, while in experiments with displacement ventilation $\dot{Q}_{vent,\,tot}$ is smaller than $\dot{Q}_{conv,\,tot}$ (excluding the first hour). Most probably this is due to a systematic error in the measurement of the temperature difference between the in- and outflowing air. The rectangular opening below the ceiling (and the temperature sensor placed in this opening) was used for the inlet air during mixing ventilation and for the outlet air during displacement ventilation. Accordingly the sensors used for the outlet air temperature during mixing ventilation were used for the inlet air during displacement ventilation. Therefore an error in this measurement might result in an increase in $\dot{Q}_{vent,\,tot}$ during mixing ventilation, but a decrease during displacement ventilation.

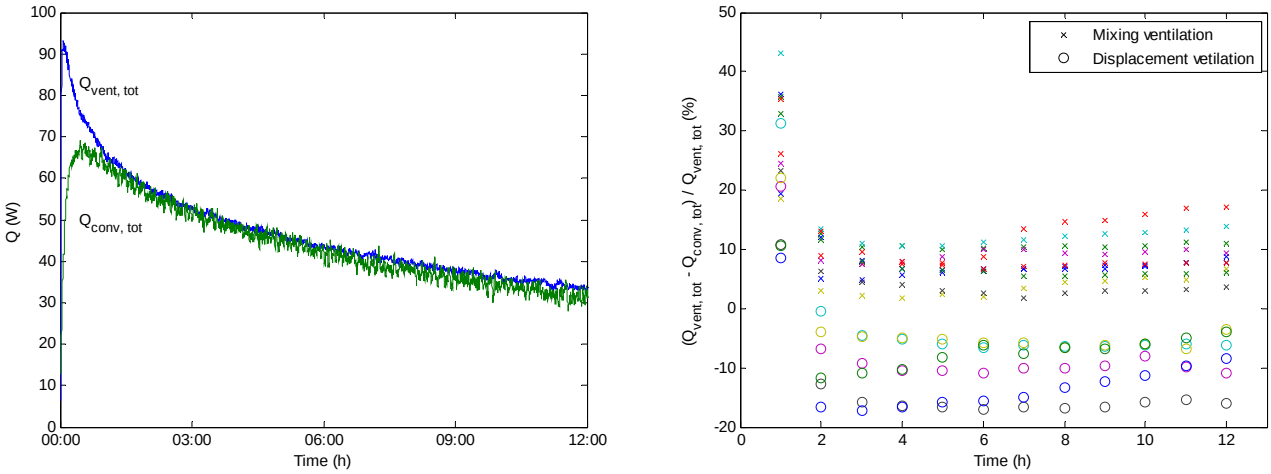

Figure 19. Total heat flow removed from the room obtained from direct measurements ($\dot{Q}_{vent,\,tot}$) and from integrating the convective heat flows over all surfaces ($\dot{Q}_{conv,\,tot}$); left: Heat flows during experiment no 4, mixing ventilation, ACR = 6.7 ACH, ΔT_0 = 2.9 K; right: Percentage of deviation, all experiments, hourly mean values.

Velocity measurements

In the first 5 experiments (no. 5, 6, 8, 9, 10 in Table 2) velocities were measured during the entire experiment. Later it turned out that the heat from the hot sphere anemometers affects the local air temperature measurements (see Figure 20). Therefore, in later experiments velocities were only measured during 10 minutes after the 12 hour measuring period.

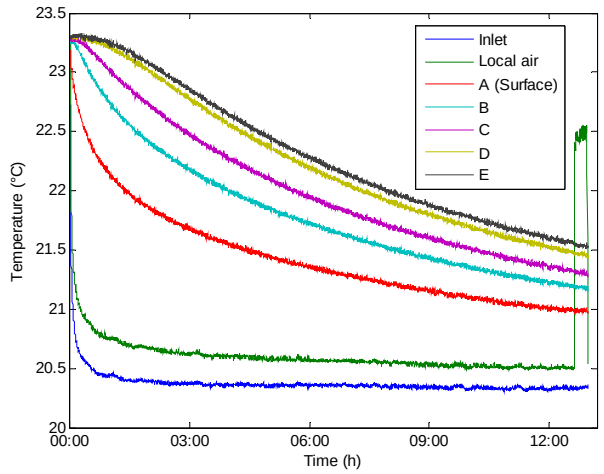

Figure 20. Increase in local air temperature during velocity measurement.

Figure 21 shows the velocities measured during experiment no. 5 with mixing ventilation with 6.8 ACH and an initial temperature difference of 6.1 K. The highest velocities occur in the centre line in front of the inlet opening (positions 3, 8, 13). The reason for the velocity at position 3 being lower than at position 8 is probably that the inlet temperature sensor partially shields the velocity sensor at position 3. The increase in the velocities at position 13 and 18 shows that the penetration of the jet changes as the room air temperature decreases. The velocity measurements also reveal that the air flow pattern is not symmetric. The velocity at position 18 is much higher than at position 17 and the velocity at position 20 is higher than at position 21. This indicates that the jet is directed to the left.

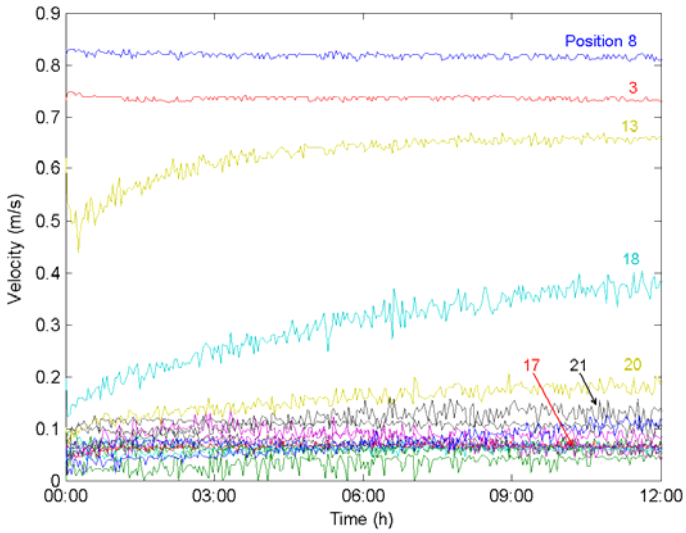

Figure 21. Velocities measured during experiment no. 5 with mixing ventilation with 6.8 ACH and an initial temperature difference of 6.1 K.

Uncertainty assessment

For each calculated quantity the uncertainty due to the uncertainty in each input parameter, *i* was calculated separately. Assuming that the uncertainties in each parameter are independent of each other, the total

uncertainty, δ was then calculated as the square root of the quadrature sum of the single uncertainties, δ_i (propagation of uncertainty):

$$\delta = \sqrt{\sum_i \delta_i^2}$$

The uncertainty in the conductive heat flux at the ceiling surfaces is estimated by variation of the input parameters of the finite difference model. Additionally to the uncertainty of the measurement equipment (± 0.086 K, [4]) the measurement of the surface temperature, *T* might be affected by radiation from other surfaces. At the ceiling this effect was assumed to be small, as the sensors were mounted before the ceiling was painted. The error was considered by adding an uncertainty depending on the radiative heat flux of ± 0.01 K/(W/m^2) (maximum ± 0.2 K for $q_{rad,max}$ = 20 W/m^2). The uncertainty in the thickness, *d* of the ceiling element was estimated as ± 3 mm and for the material properties the uncertainties given in Table 1 were used. Additionally uncertainties in the conductivity, λ and the volumetric heat capacity, ρc of the gypsum boards were considered (see Table 1).

Exemplarily, the results for two cases with a small and a high heat flux are shown in Figure 22. The cumulative distribution function of the uncertainty in the total heat flow from the ceiling during all experiments due to measurement errors is shown in Figure 23. During 95 % of the time, the uncertainty is below 10 %.

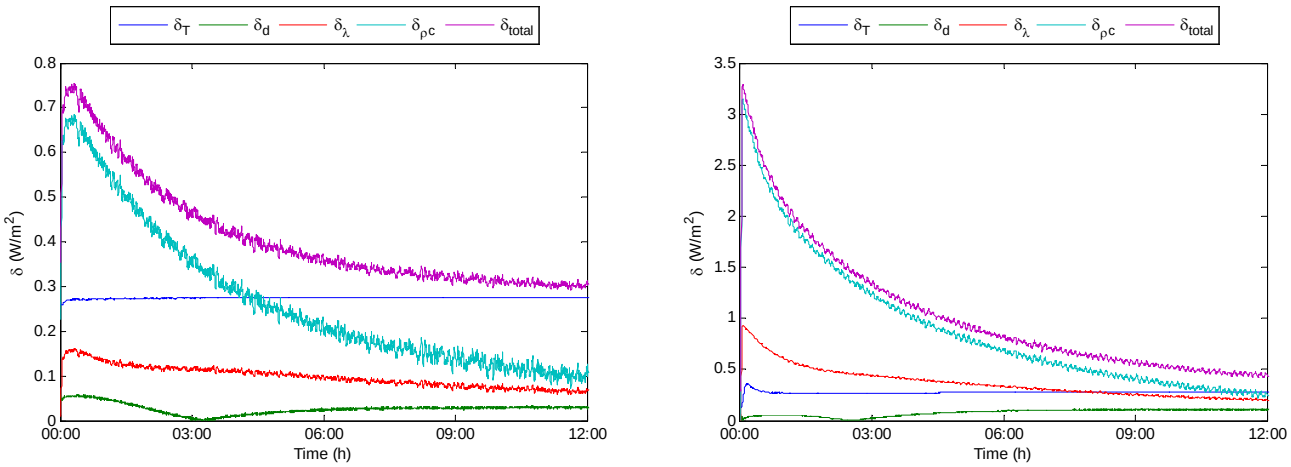

Figure 22. Uncertainty in the conductive heat flux at the ceiling due to different input parameters; left: small heat flux (experiment no. 4, position 8); right: high heat flux (experiment no. 10, position 8).

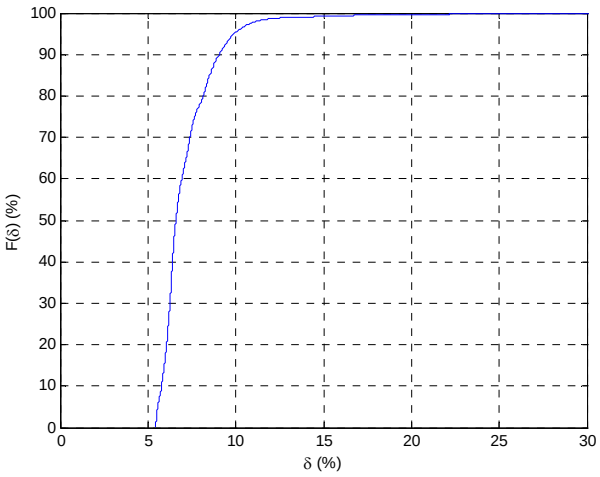

Figure 23. Cumulative distribution function of the uncertainty in the heat flux at the ceiling due to measurement errors.

An additional uncertainty is introduced by the integration of the heat flux over the ceiling surface. This error is largest for cases with an inhomogeneous heat flux, i.e. in cases with a jet flowing along the ceiling. In the base case the previously calculated heat flux at each measuring point was multiplied by the corresponding area as shown in Figure 8. This corresponds to a linear interpolation between the measuring points. To estimate the uncertainty, the profile in each row (positions 1 to 5, 6 to 10, 11 to 15, 16 to 19 and 20 to 22) was varied as shown in Figure 24 (left). For each section the minimum and maximum heat flux was calculated as follows:

$$\dot{q}_{\min,i} = \min\left(\frac{\dot{q}_{i-1}+\dot{q}_i}{2}, \dot{q}_i, \frac{\dot{q}_i+\dot{q}_{i+1}}{2}\right); \quad \dot{q}_{\max,i} = \max\left(\frac{\dot{q}_{i-1}+\dot{q}_i}{2}, \dot{q}_i, \frac{\dot{q}_i+\dot{q}_{i+1}}{2}\right)$$

The resulting uncertainty in the total conductive heat flux at the ceiling during experiment no. 10 is shown in Figure 24 (right). The uncertainty is largest in the beginning of the experiment and decreases as the heat flux becomes more homogeneous (cf. Figure 17). The cumulative distribution function of the uncertainty resulting from integrating the heat flux over the ceiling surface during all experiments is shown in Figure 25 (left). During 95 % of the time, the uncertainty is below ± 10 %.

For each time step the total uncertainty was calculated as the square root of the quadrature sum of the uncertainty due to measurement errors and the uncertainty resulting from the integration over the ceiling surface. The cumulative distribution function of the uncertainty in the total heat flow from the ceiling is shown in Figure 25 (right). During 95 % of the time, the uncertainty is below ± 13 %.

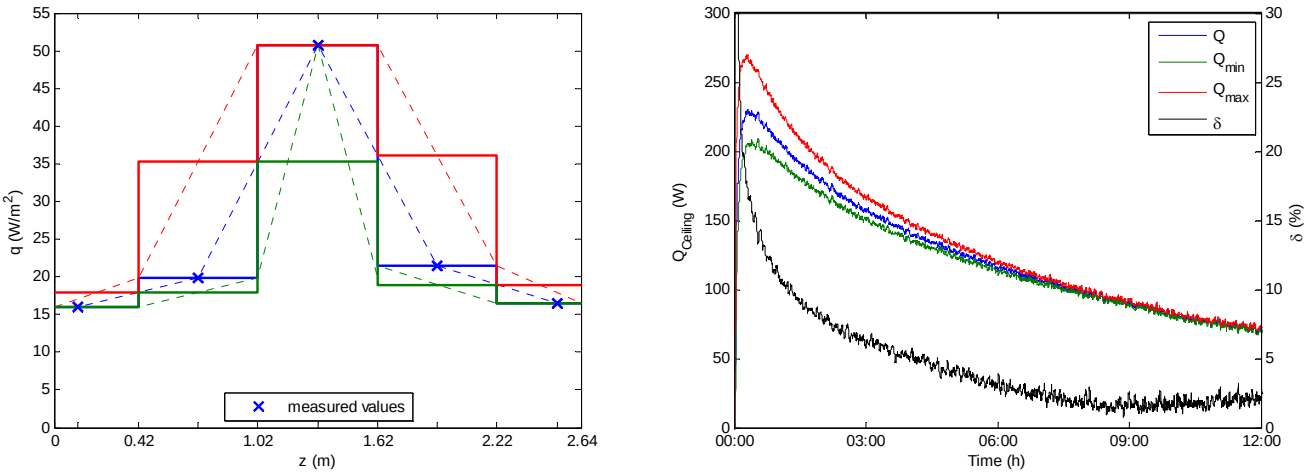

Figure 24. Uncertainty resulting from the integration of the heat flux over the ceiling surface; left: Different heat flux profiles (dotted lines give the same result as the step curves; congruent triangles); right: Resulting uncertainty in the total conductive heat flux at the ceiling during experiment no. 10.

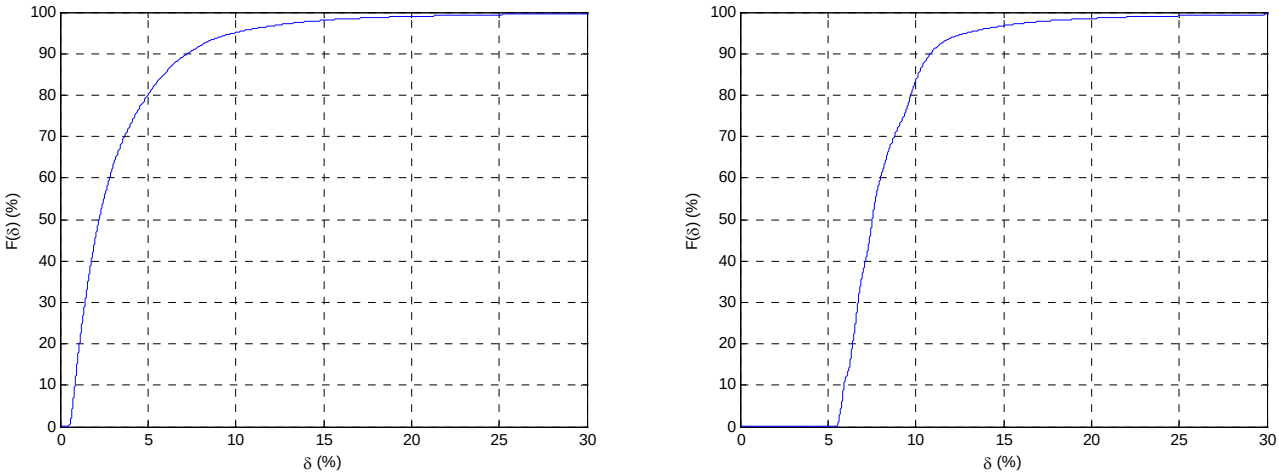

Figure 25. Cumulative distribution functions of the uncertainty resulting from integrating the heat flux over the ceiling surface (left) and the total uncertainty in the total heat flow from the ceiling (right).

Also the uncertainty in the conductive heat flux at the floor and wall surfaces was assessed by variation of the input parameters of the finite difference model. In this case the temperature at the internal surface and the heat flux at the external surface were used as boundary conditions. As the temperature difference ΔT, used to calculate the external heat flux, was measured with a thermopile made of 4 thermocouples, and radiation effects can be excluded, the uncertainty was estimated as ± 0.05 K. The uncertainty in the surface temperature, T_{Surf} due to radiation effects was assumed to be higher at the walls than at the ceiling. The error was considered by adding an uncertainty depending on the radiative heat flux of ± 0.042 K/(W/m^2) (maximum ± 0.5 K for $q_{rad,max}$ = 12 W/m^2). The uncertainty in the distance, d_1 between the two sensors measuring the temperature difference was estimated as ± 2 mm. The distance, d_2 was assumed to be 115 ± 15 mm (Figure 27). This also includes the uncertainty emerging from a non-linear temperature profile over d_1. The uncertainties in the conductivity, λ and the volumetric heat capacity, ρc of the EPS were assumed as given in Table 1.

Exemplarily, the results for two cases with a small and a high heat flux are shown in Figure 27. The cumulative distribution function of the uncertainty in the heat flow from the walls and the floor due to measurement errors is shown in Figure 28. Here in some cases a high relative uncertainty occurs due to small absolute heat flows. As the heat flows at the floor and walls are generally small compared to the heat flow from the ceiling, this uncertainty does not affect the total heat flow from the whole room too much. The uncertainty resulting from the integration of the heat flow over the floor and wall surfaces was estimated as ± 10 %.

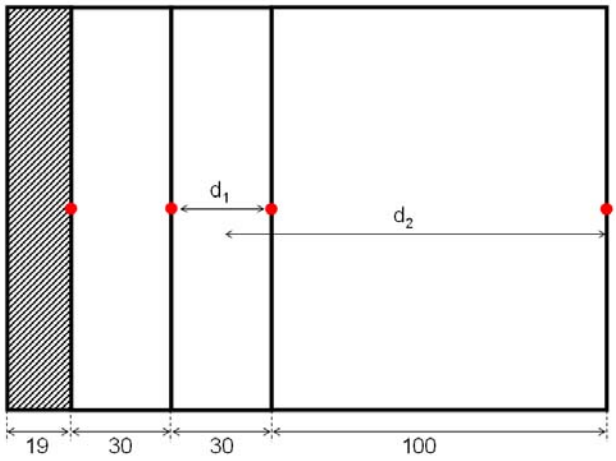

Figure 26. Distances d_1 and d_2 used for the calculation of the surface heat flux at the floor and walls.

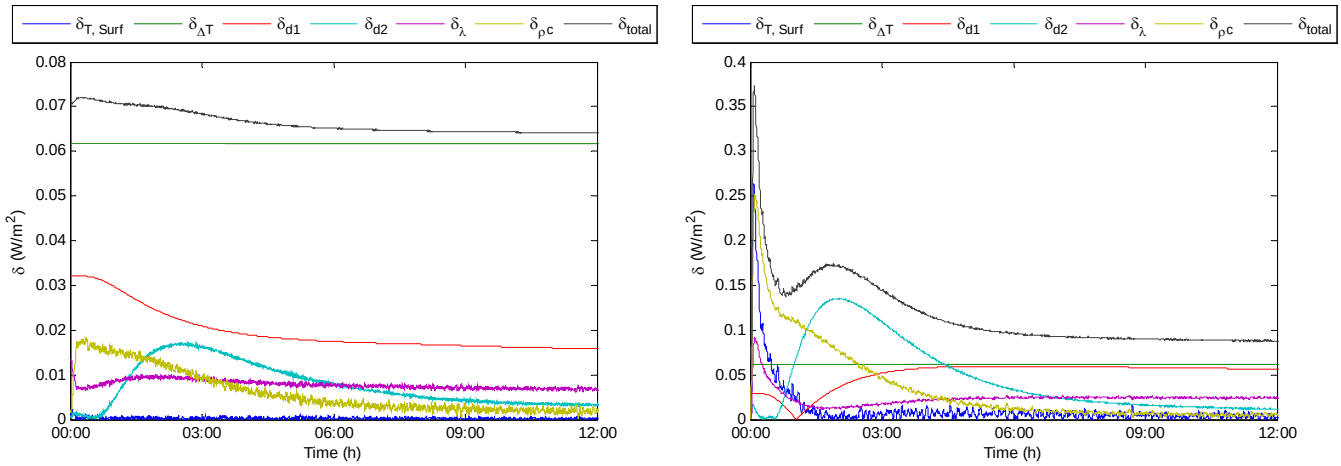

Figure 27. Uncertainty in the conductive heat flux at the floor due to different input parameters; left: small heat flux (experiment no. 4, central measuring point at the floor); right: high heat flux (experiment no. 16, central measuring point at the floor).

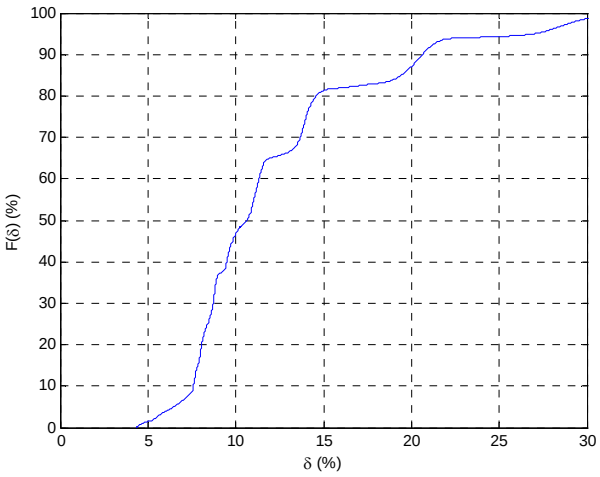

Figure 28. Cumulative distribution functions of the uncertainty in the conductive heat flux at the floor and wall surfaces due to measurement errors.

To assess the uncertainty in the total conductive heat flow at all room surfaces the absolute uncertainties in the heat flows at the ceiling and the other surfaces were summed up and put into relation to the total heat flow. The cumulative distribution function of the uncertainty in the total conductive heat flow from all room surfaces during all experiments is shown in Figure 29. During 95 % of the time, the uncertainty is below ± 16 %.

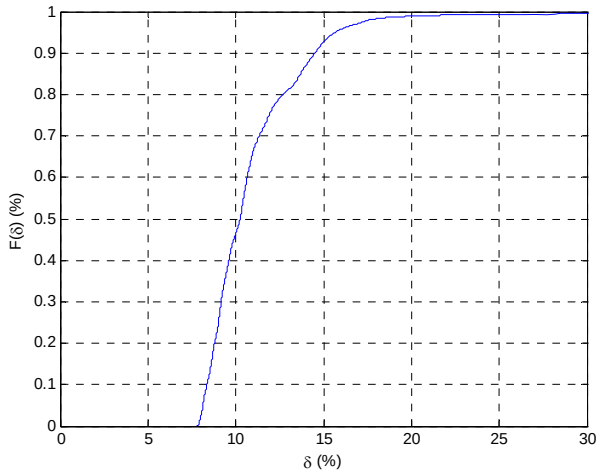

Figure 29. Cumulative distribution function of the uncertainty in the total conductive heat flow from all room surfaces.

For the calculation of the radiative heat flows it is assumed that the surface temperature is homogeneous in each section (22 sections at the ceiling and 3 sections at each wall and floor surface). To estimate the uncertainty introduced by this assumption, the error in averaging the ceiling surface temperature is assessed applying the same method as for the integration of the conduction heat flow (cf. Figure 24, left). The maximum error was ± 0.4 K corresponding to ± 5 % (relative to ΔT_0). The total uncertainty in the temperature difference was estimated as ± 10 %. The sensitivity of the radiative heat flow on uncertainties in the temperature difference and the emissivities (± 5 %) was assumed to be linear. The uncertainties in the

Stefan-Boltzmann constant and the geometric parameters were neglected. For the total uncertainty in the radiative heat flow follows:

$$\delta_{\dot{Q},rad} = \sqrt{\delta_{\varepsilon 1}{}^2 + \delta_{\varepsilon 2}{}^2 + \delta_{\Delta T}{}^2} = \sqrt{5^2 + 5^2 + 10^2} = \pm 12\%$$

As the sum of all radiative heat flows at all room surfaces is zero, the total convective heat flow from the room equals the total conductive heat flow and the uncertainty is also the same. The uncertainty in the convective heat flow from the ceiling was assessed as the square root of quadrature sum of the uncertainties in the conductive and radiative heat flows. The cumulative distribution functions of the absolute and relative uncertainty in the convective heat flow from the ceiling are shown in Figure 30. The calculation of the convective heat flow as difference between conduction and radiation, results in a high relative uncertainty (Figure 30, left). During 95 % of the time, the absolute uncertainty is below ± 2.2 W/m^2 (Figure 30, right).

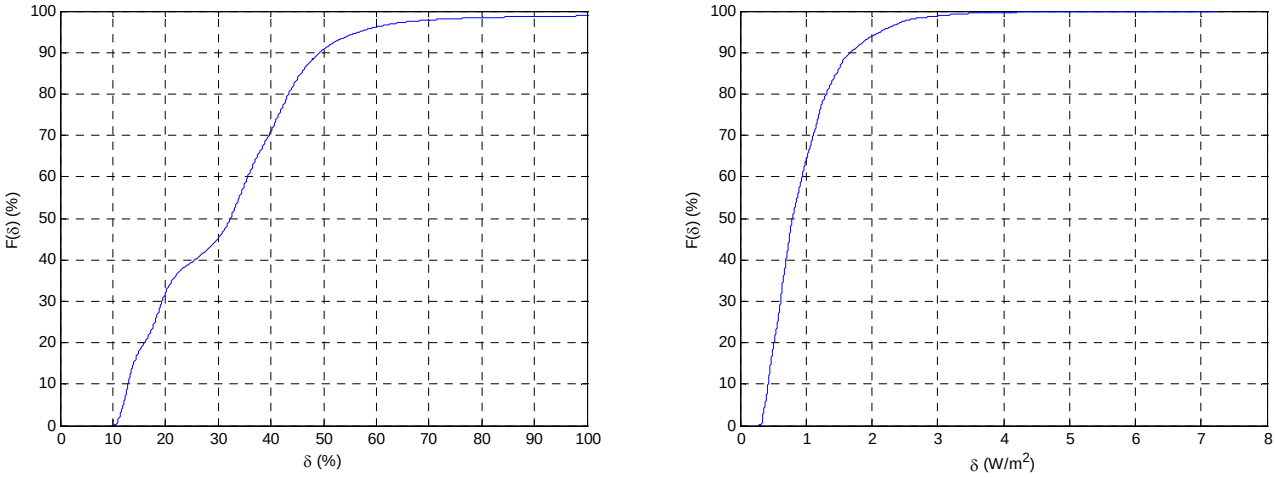

Figure 30. Cumulative distribution functions of the uncertainty in the mean convective heat flux from the ceiling; left: relative (%), right: absolute (W/m^2).

The ratio between the convective and the total heat flow from the ceiling, γ is defined as:

$$\gamma = \frac{\dot{Q}_{conv,Ceiling}}{\dot{Q}_{cond,Ceiling}} = 1 - \frac{\dot{Q}_{rad,Ceiling}}{\dot{Q}_{cond,Ceiling}}$$

The uncertainty in γ was calculated based on the uncertainties in $\dot{Q}_{rad,Ceiling}$ and $\dot{Q}_{cond,Ceiling}$. The cumulative distribution function of the absolute uncertainty in the convection ratio γ is shown in Figure 31. During 95 % of the time, the absolute uncertainty is below ± 0.11.

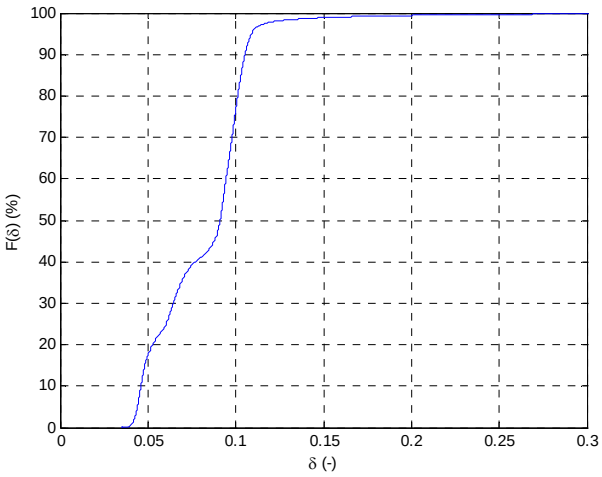

Figure 31. Cumulative distribution function of the absolute uncertainty in the convection ratio γ at the ceiling.

The total heat flow removed from the room was calculated based on the temperature difference between the in- and outflowing air and the air flow rate. The difference between the inlet and outlet air temperature was measured by a thermopile consisting of two thermocouples. Therefore the uncertainty is assumed to be dominated by radiation effects and was estimated as ± 10 %. The accuracy of the air flow measurement is given by the manufacturer of the orifice as ± 5 %. The uncertainties in the density and the thermal capacity of the air were estimated as ± 3 % and ± 1 %, respectively. For the uncertainty in the total heat flow removed by ventilation follows:

$$\delta_{\dot{Q},tot,vent} = \sqrt{\delta_{\dot{V},Air}{}^2 + \delta_{\rho,Air}{}^2 + \delta_{c_p,Air}{}^2 + \delta_{\Delta T}{}^2} = \sqrt{5^2 + 3^2 + 1^2 + 10^2} = \pm 12\,\%$$

The ventilation efficiency, η was defined as:

$$\eta = \frac{T_{Outlet} - T_{Inlet}}{\overline{T}_{Surface} - T_{Inlet}}$$

The uncertainty in the difference between the inlet and outlet air temperature was again estimated as ± 10 %. For the difference between the average room surface temperature and the inlet air temperature the uncertainty was estimated as ± 10 %. For the ventilation efficiency, η follows:

$$\delta_{\eta} = \sqrt{10^2 + 10^2} = \pm 14\,\%$$

Discussion and conclusion

A test room was equipped with temperature and air flow velocity sensors for a detailed analysis of heat transfer during night-time ventilation. Temperatures were measured at 22 points at the ceiling and at 3 points at each wall and floor surface. From the measured temperatures surface heat flows were calculated using a 1-dimensional finite difference model. The uncertainty in the conductive heat flow at the ceiling due to measurement errors was estimated as ± 10 %.

Additional uncertainty in the same order of magnitude is introduced by the integration of the heat flow over the ceiling surface (22 sections). Alternatively, a 3-dimensional finite difference model could be used to

determine the 3-dimensional temperature field in the ceiling element and thus the surface heat flow with a higher resolution. However, as the jet at the ceiling might cause a discontinuous surface temperature profile, the application of a 3-dimensional model is not expected to improve the accuracy significantly.

The radiative heat flows between different surfaces were determined from the measured surface temperatures. The difference between conduction and radiation then yielded the convective heat flow at each surface section. Integration over all surfaces results in the total heat flow discharged from the room.

The uncertainty in the total heat flow discharged from the room yielded from surface heat flow measurements was estimated as ± 16 %. The uncertainty in the heat flow resulting from in-/ outflowing air temperature and mass flow measurements was estimated as ± 12 %. Considering these uncertainties yielded overlapping uncertainty bands for all experiments.

Although there are considerable uncertainties, the presented method is regarded to be suitable to investigate surface heat transfer during night-time ventilation.

References

[1] Jensen R L. Modelling of natural ventilation and night cooling – by the Loop Equation Method. PhD-thesis, Aalborg University, Department of Civil Engineering, Hybrid Ventilation Centre, 2005 (in Danish).

[2] EN 12524:2000. Building materials and products - Hygrothermal properties - Tabulated design values. German version.

[3] Bavarian center for applied energy research (ZAE Bayern) Bestimmung des Emissionsgrades von einer EPS Probe. Report ZAE 2-0808-05, 2008 (in German).

[4] Artmann N, Vonbank R, Jensen R L. Temperature measurements using type K thermocouples and the Fluke Helios Plus 2287A data logger. Internal report, Aalborg University, 2008

[5] Grant Data Acquisition. Technical notes – Squirrel 2020 / 2040 Full Technical Specification and Accessories. Downloaded from http://www.grant.co.uk June 2008.

[6] Ehlert J R, Smith T F. View factors for perpendicular and parallel rectangular plates. Journal of thermophysics and heat transfer 1993, 7 (1), pp. 173-174.

Appendix

Table A1. Sensor configuration for Helios data loggers.

Logger	Channel	Inputblock		ch	Comp. Box		Cable Nr.	High	Low	Location
283	1	1	Isothermal	0	8A	A0	1A	brown	blue	Ceiling 1 A
283	2	1	Isothermal	1	8A	A1	1B	brown	blue	Ceiling 1 B
283	3	1	Isothermal	2	8A	A2	1C	brown	blue	Ceiling 1 C
283	4	1	Isothermal	3	8A	A3	1D	brown	blue	Ceiling 1 D
283	5	1	Isothermal	4	8A	A4	1E	brown	blue	Ceiling 1 E
283	6	1	Isothermal	5	8A	A5	2A	green	white	Ceiling 2 A
283	7	1	Isothermal	6	8A	A6	2B	green	white	Ceiling 2 B
283	8	1	Isothermal	7	8A	A7	2C	green	white	Ceiling 2 C
283	9	1	Isothermal	8	8A	A8	2D	green	white	Ceiling 2 D
283	10	1	Isothermal	9	8A	A9	2E	green	white	Ceiling 2 E
283	11	1	Isothermal	10	8B	B0	3A	brown	blue	Ceiling 3 A
283	12	1	Isothermal	11	8B	B1	3B	brown	blue	Ceiling 3 B
283	13	1	Isothermal	12	8B	B2	3C	brown	blue	Ceiling 3 C
283	14	1	Isothermal	13	8B	B3	3D	brown	blue	Ceiling 3 D
283	15	1	Isothermal	14	8B	B4	3E	brown	blue	Ceiling 3 E
283	16	1	Isothermal	15	8B	B5	4A	green	white	Ceiling 4 A
283	17	1	Isothermal	16	8B	B6	4B	green	white	Ceiling 4 B
283	18	1	Isothermal	17	8B	B7	4C	green	white	Ceiling 4 C
283	19	1	Isothermal	18	8B	B8	4D	green	white	Ceiling 4 D
283	20	1	Isothermal	19	8B	B9	4E	green	white	Ceiling 4 E
Logger	**Channel**	**Inputblock**		**ch**	**Comp. Box**		**Cable Nr.**	**High**	**Low**	**Location**
283	21	2	Isothermal	0	1A	A0	5A	brown	blue	Ceiling 5 A
283	22	2	Isothermal	1	1A	A1	5B	brown	blue	Ceiling 5 B
283	23	2	Isothermal	2	1A	A2	5C	brown	blue	Ceiling 5 C
283	24	2	Isothermal	3	1A	A3	5D	brown	blue	Ceiling 5 D
283	25	2	Isothermal	4	1A	A4	5E	brown	blue	Ceiling 5 E
283	26	2	Isothermal	5	1A	A5	6A	green	white	Ceiling 6 A
283	27	2	Isothermal	6	1A	A6	6B	green	white	Ceiling 6 B
283	28	2	Isothermal	7	1A	A7	6C	green	white	Ceiling 6 C
283	29	2	Isothermal	8	1A	A8	6D	green	white	Ceiling 6 D
283	30	2	Isothermal	9	1A	A9	6E	green	white	Ceiling 6 E
283	31	2	Isothermal	10	1B	B0	7A	green	white	Ceiling 7 A
283	32	2	Isothermal	11	1B	B1	7B	green	white	Ceiling 7 B
283	33	2	Isothermal	12	1B	B2	7C	green	white	Ceiling 7 C
283	34	2	Isothermal	13	1B	B3	7D	green	white	Ceiling 7 D
283	35	2	Isothermal	14	1B	B4	7E	green	white	Ceiling 7 E
283	36	2	Isothermal	15	1B	B5	8A	green	white	Ceiling 8 A
283	37	2	Isothermal	16	1B	B6	8B	green	white	Ceiling 8 B
283	38	2	Isothermal	17	1B	B7	8C	green	white	Ceiling 8 C
283	39	2	Isothermal	18	1B	B8	8D	green	white	Ceiling 8 D
283	40	2	Isothermal	19	1B	B9	8E	green	white	Ceiling 8 E
Logger	**Channel**	**Inputblock**		**ch**	**Comp. Box**		**Cable Nr.**	**High**	**Low**	**Location**
283	41	3	Isothermal	0	2A	A0	9A	green	white	Ceiling 9 A
283	42	3	Isothermal	1	2A	A1	9B	green	white	Ceiling 9 B
283	43	3	Isothermal	2	2A	A2	9C	green	white	Ceiling 9 C
283	44	3	Isothermal	3	2A	A3	9D	green	white	Ceiling 9 D
283	45	3	Isothermal	4	2A	A4	9E	green	white	Ceiling 9 E
283	46	3	Isothermal	5	2A	A5	10A	green	white	Ceiling 10 A
283	47	3	Isothermal	6	2A	A6	10B	green	white	Ceiling 10 B
283	48	3	Isothermal	7	2A	A7	10C	green	white	Ceiling 10 C
283	49	3	Isothermal	8	2A	A8	10D	green	white	Ceiling 10 D
283	50	3	Isothermal	9	2A	A9	10E	green	white	Ceiling 10 E
283	51	3	Isothermal	10	2B	B0	1	green	white	Surface Low X, bottom
283	52	3	Isothermal	11	2B	B1	2	green	white	Surface High X, bottom
283	53	3	Isothermal	12	2B	B2	3	green	white	Surface Low Z, bottom
283	54	3	Isothermal	13	2B	B3	4	green	white	Surface High Z, bottom
283	55	3	Isothermal	14	2B	B4	5	green	white	Surface Low X, centre
283	56	3	Isothermal	15	2B	B5	6	green	white	Surface High X, centre
283	57	3	Isothermal	16	2B	B6	7	green	white	Surface Low Z, centre
283	58	3	Isothermal	17	2B	B7	8	green	white	Surface High Z, centre
283	59	3	Isothermal	18	2B	B8	9	green	white	Surface Low X, top
283	60	3	Isothermal	19	2B	B9	10	green	white	Surface High X, top

Logger	Channel	Inputblock		ch	Comp. Box		Cable Nr.	High	Low	Location
283	61	4	Sullins	0	6B	B0	11	green	white	Surface Low Z, top
283	62	4	Sullins	1	6B	B1	12	green	white	Surface High Z, top
283	63	4	Sullins	2	6B	B2	13	green	white	Surface Floor, low x
283	64	4	Sullins	3	6B	B3	14	green	white	Surface Floor, centre
283	65	4	Sullins	4	6B	B4	15	green	white	Surface Floor, high x
283	66	4	Sullins	5	6B	B5	A1	green	white	Air Low X, bottom
283	67	4	Sullins	6	6B	B6	A2	green	white	Air High X, bottom
283	68	4	Sullins	7	6B	B7	A3	green	white	Air Low Z, bottom
283	69	4	Sullins	8	6B	B8	A4	green	white	Air High Z, bottom
283	70	4	Sullins	9	6B	B9	A5	green	white	Air Low X, centre
283	71	4	Sullins	10	7A	A0	A6	green	white	Air High X, centre
283	72	4	Sullins	11	7A	A1	A7	green	white	Air Low Z, centre
283	73	4	Sullins	12	7A	A2	A8	green	white	Air High Z, centre
283	74	4	Sullins	13	7A	A3	A9	green	white	Air Low X, top
283	75	4	Sullins	14	7A	A4	A10	green	white	Air High X, top
283	76	4	Sullins	15	7A	A5	A11	green	white	Air Low Z, top
283	77	4	Sullins	16	7A	A6	A12	green	white	Air High Z, top
283	78	4	Sullins	17	7A	A7	A13	green	white	Air Floor, low x
283	79	4	Sullins	18	7A	A8	A14	green	white	Air Floor, centre
283	80	4	Sullins	19	7A	A9	A15	green	white	Air Floor, high x
Logger	**Channel**	**Inputblock**		**ch**	**Comp. Box**		**Cable Nr.**	**High**	**Low**	**Location**
283	81	5	Voltage	0			1	blue	green	ΔT Low X, bottom
283	82	5	Voltage	1			2	blue	green	ΔT High X, bottom
283	83	5	Voltage	2			3	blue	green	ΔT Low Z, bottom
283	84	5	Voltage	3			4	blue	green	ΔT High Z, bottom
283	85	5	Voltage	4			5	yellow	orange	ΔT Low X, centre
283	86	5	Voltage	5			6	yellow	orange	ΔT High X, centre
283	87	5	Voltage	6			7	yellow	orange	ΔT Low Z, centre
283	88	5	Voltage	7			8	yellow	orange	ΔT High Z, centre
283	89	5	Voltage	8			9	red	brown	ΔT Low X, top
283	90	5	Voltage	9			10	red	brown	ΔT High X, top
283	91	5	Voltage	10			11	red	brown	ΔT Low Z, top
283	92	5	Voltage	11			12	red	brown	ΔT High Z, top
283	93	5	Voltage	12			13	blue	green	ΔT Floor, low x
283	94	5	Voltage	13			14	yellow	orange	ΔT Floor, centre
283	95	5	Voltage	14			15	red	brown	ΔT Floor, high x
283	96	5	Voltage	15			16	black	white	ΔT In- Outlet, low z
283	97	5	Voltage	16			17	grey	lilac	ΔT In- Outlet, high z
283	98	5	Voltage	17	7B	B0	In	green	white	Inlet
283	99	5	Voltage	18	7B	B1	43	red	green	Ice point 41
283	100	5	Voltage	19	7B	B2	44	red	green	Ice point 42
Logger	**Channel**	**Inputblock**		**ch**	**Comp. Box**		**Cable Nr.**	**High**	**Low**	**Location**
233	1	1	Isothermal	0	3A	A0	11A	green	white	Ceiling 11 A
233	2	1	Isothermal	1	3A	A1	11B	green	white	Ceiling 11 B
233	3	1	Isothermal	2	3A	A2	11C	green	white	Ceiling 11 C
233	4	1	Isothermal	3	3A	A3	11D	green	white	Ceiling 11 D
233	5	1	Isothermal	4	3A	A4	11E	green	white	Ceiling 11 E
233	6	1	Isothermal	5	3A	A5	12A	brown	blue	Ceiling 12 A
233	7	1	Isothermal	6	3A	A6	12B	brown	blue	Ceiling 12 B
233	8	1	Isothermal	7	3A	A7	12C	brown	blue	Ceiling 12 C
233	9	1	Isothermal	8	3A	A8	12D	brown	blue	Ceiling 12 D
233	10	1	Isothermal	9	3A	A9	12E	brown	blue	Ceiling 12 E
233	11	1	Isothermal	10	3B	B0	13A	brown	blue	Ceiling 13 A
233	12	1	Isothermal	11	3B	B1	13B	brown	blue	Ceiling 13 B
233	13	1	Isothermal	12	3B	B2	13C	brown	blue	Ceiling 13 C
233	14	1	Isothermal	13	3B	B3	13D	brown	blue	Ceiling 13 D
233	15	1	Isothermal	14	3B	B4	13E	brown	blue	Ceiling 13 E
233	16	1	Isothermal	15	3B	B5	14A	green	white	Ceiling 14 A
233	17	1	Isothermal	16	3B	B6	14B	brown	blue	Ceiling 14 B
233	18	1	Isothermal	17	3B	B7	14C	brown	blue	Ceiling 14 C
233	19	1	Isothermal	18	3B	B8	14D	brown	blue	Ceiling 14 D
233	20	1	Isothermal	19	3B	B9	14E	brown	blue	Ceiling 14 E

Logger	Channel	Inputblock		ch	Comp. Box		Cable Nr.	High	Low	Location
233	21	2	Isothermal	0	4A	A0	15A	green	white	Ceiling 15
233	22	2	Isothermal	1	4A	A1	15B	green	white	Ceiling 15
233	23	2	Isothermal	2	4A	A2	15C	green	white	Ceiling 15
233	24	2	Isothermal	3	4A	A3	15D	green	white	Ceiling 15
233	25	2	Isothermal	4	4A	A4	15E	green	white	Ceiling 15
233	26	2	Isothermal	5	4A	A5	16A	brown	blue	Ceiling 16
233	27	2	Isothermal	6	4A	A6	16B	brown	blue	Ceiling 16
233	28	2	Isothermal	7	4A	A7	16C	brown	blue	Ceiling 16
233	29	2	Isothermal	8	4A	A8	16D	brown	blue	Ceiling 16
233	30	2	Isothermal	9	4A	A9	16E	brown	blue	Ceiling 16
233	31	2	Isothermal	10	4B	B0	17A	brown	blue	Ceiling 17
233	32	2	Isothermal	11	4B	B1	17B	brown	blue	Ceiling 17
233	33	2	Isothermal	12	4B	B2	17C	brown	blue	Ceiling 17
233	34	2	Isothermal	13	4B	B3	17D	brown	blue	Ceiling 17
233	35	2	Isothermal	14	4B	B4	17E	brown	blue	Ceiling 17
233	36	2	Isothermal	15	4B	B5	18A	brown	blue	Ceiling 18
233	37	2	Isothermal	16	4B	B6	18B	brown	blue	Ceiling 18
233	38	2	Isothermal	17	4B	B7	18C	brown	blue	Ceiling 18
233	39	2	Isothermal	18	4B	B8	18D	brown	blue	Ceiling 18
233	40	2	Isothermal	19	4B	B9	18E	brown	blue	Ceiling 18
Logger	**Channel**	**Inputblock**		**ch**	**Comp. Box**		**Cable Nr.**	**High**	**Low**	**Location**
233	41	3	Isothermal	0	5A	A0	19A	brown	blue	Ceiling 19
233	42	3	Isothermal	1	5A	A1	19B	brown	blue	Ceiling 19
233	43	3	Isothermal	2	5A	A2	19C	brown	blue	Ceiling 19
233	44	3	Isothermal	3	5A	A3	19D	brown	blue	Ceiling 19
233	45	3	Isothermal	4	5A	A4	19E	brown	blue	Ceiling 19
233	46	3	Isothermal	5	5A	A5	20A	green	white	Ceiling 20
233	47	3	Isothermal	6	5A	A6	20B	green	white	Ceiling 20
233	48	3	Isothermal	7	5A	A7	20C	green	white	Ceiling 20
233	49	3	Isothermal	8	5A	A8	20D	green	white	Ceiling 20
233	50	3	Isothermal	9	5A	A9	20E	green	white	Ceiling 20
233	51	3	Isothermal	10	5B	B0	21A	brown	blue	Ceiling 21
233	52	3	Isothermal	11	5B	B1	21B	brown	blue	Ceiling 21
233	53	3	Isothermal	12	5B	B2	21C	brown	blue	Ceiling 21
233	54	3	Isothermal	13	5B	B3	21D	brown	blue	Ceiling 21
233	55	3	Isothermal	14	5B	B4	21E	brown	blue	Ceiling 21
233	56	3	Isothermal	15	5B	B5	22A	green	white	Ceiling 22
233	57	3	Isothermal	16	5B	B6	22B	green	white	Ceiling 22
233	58	3	Isothermal	17	5B	B7	22C	green	white	Ceiling 22
233	59	3	Isothermal	18	5B	B8	22D	green	white	Ceiling 22
233	60	3	Isothermal	19	5B	B9	22E	green	white	Ceiling 22
Logger	**Channel**	**Inputblock**		**ch**	**Comp. Box**		**Cable Nr.**	**High**	**Low**	**Location**
233	61	4	Isothermal	0	I. p. 1	1	1	red	green	Air Ceiling 1
233	62	4	Isothermal	1	I. p. 1	2	2	red	green	Air Ceiling 2
233	63	4	Isothermal	2	I. p. 1	3	3	red	green	Air Ceiling 3
233	64	4	Isothermal	3	I. p. 1	4	4	red	green	Air Ceiling 4
233	65	4	Isothermal	4	I. p. 1	5	5	red	green	Air Ceiling 5
233	66	4	Isothermal	5	I. p. 1	6	6	red	green	Air Ceiling 6
233	67	4	Isothermal	6	I. p. 1	7	7	red	green	Air Ceiling 7
233	68	4	Isothermal	7	I. p. 1	8	8	red	green	Air Ceiling 8
233	69	4	Isothermal	8	I. p. 1	9	9	red	green	Air Ceiling 9
233	70	4	Isothermal	9	I. p. 1	10	10	red	green	Air Ceiling 10
233	71	4	Isothermal	10	I. p. 2	11	11	red	green	Air Ceiling 11
233	72	4	Isothermal	11	I. p. 2	12	12	red	green	Air Ceiling 12
233	73	4	Isothermal	12	I. p. 2	13	13	red	green	Air Ceiling 13
233	74	4	Isothermal	13	I. p. 2	14	14	red	green	Air Ceiling 14
233	75	4	Isothermal	14	I. p. 2	15	15	red	green	Air Ceiling 15
233	76	4	Isothermal	15	I. p. 2	16	16	red	green	Air Ceiling 16
233	77	4	Isothermal	16	I. p. 2	17	17	red	green	Air Ceiling 17
233	78	4	Isothermal	17	I. p. 2	18	18	red	green	Air Ceiling 18
233	79	4	Isothermal	18	I. p. 2	19	19	red	green	Air Ceiling 19
233	80	4	Isothermal	19	I. p. 2	20	20	red	green	Air Ceiling 20

Logger	Channel	Inputblock		ch	Comp. Box		Cable Nr.	High	Low	Location
233	81	5	Isothermal	0	I. p. 3	21	21	red	green	Air Ceiling 21
233	82	5	Isothermal	1	I. p. 3	22	22	red	green	Air Ceiling 22
233	83	5	Isothermal	2	I. p. 3	23	23	red	green	Air A 0.1 m
233	84	5	Isothermal	3	I. p. 3	24	24	red	green	Air A 1.1 m
233	85	5	Isothermal	4	I. p. 3	25	25	red	green	Air A 1.7 m
233	86	5	Isothermal	5	I. p. 3	26	26	red	green	Air A 2.6 m
233	87	5	Isothermal	6	I. p. 3	27	27	red	green	Air B 0.1 m
233	88	5	Isothermal	7	I. p. 3	28	28	red	green	Air B 1.1 m
233	89	5	Isothermal	8	I. p. 3	29	29	red	green	Air B 1.7 m
233	90	5	Isothermal	9	I. p. 3	30	30	red	green	Air B 2.6 m
233	91	5	Isothermal	10	I. p. 4	31	31	red	green	Air C 0.1 m
233	92	5	Isothermal	11	I. p. 4	32	32	red	green	Air C 1.1 m
233	93	5	Isothermal	12	I. p. 4	33	33	red	green	Air C 1.7 m
233	94	5	Isothermal	13	I. p. 4	34	34	red	green	Air C 2.6 m
233	95	5	Isothermal	14	I. p. 4	35	35	red	green	Air C 2.9 m
233	96	5	Isothermal	15	I. p. 4	36	36	red	green	Outlet Low Z
233	97	5	Isothermal	16	I. p. 4	37	37	red	green	Outlet High Z
233	98	5	Isothermal	17	6A	A0	-			
233	99	5	Isothermal	18	6A	A1	43	red	green	Ice point 43
233	100	5	Isothermal	19	6A	A2	44	red	green	Ice point 44

Table A2. Sensor configuration for Grant Squirrel data logger.

Channel	Plug	Block	Pins	Type	Location	x (m) *	y (m) *	z (m) *
1	1	A	1-5	thin	Wall Low X, bottom	0.000	0.720	1.480
2	1	A	2-5	thin	Wall High X, bottom	3.490	0.720	1.480
3	1	A	3-5	thin	Wall Low Z, bottom	1.750	0.720	0.000
4	1	A	4-5	thin	Wall High Z, bottom	2.000	0.720	2.960
5	2	B	1-5	thin	Wall Low X, centre	0.000	1.700	1.480
6	2	B	2-5	thin	Wall High X, centre	3.490	1.700	1.480
7	2	B	3-5	thin	Wall Low Z, centre	1.750	1.700	0.000
8	2	B	4-5	thin	Wall High Z, centre	2.000	1.700	2.960
9	3	C	1-5	thin	Wall Low X, top	0.000	2.670	1.480
10	3	C	2-5	thin	Wall High X, top	3.490	2.670	1.480
11	3	C	3-5	thin	Wall Low Z, top	1.750	2.670	0.000
12	3	C	4-5	thin	Wall High Z, top	2.000	2.670	2.960
13	4	D	1-5	thin	Floor, low x	0.690	0.000	1.480
14	4	D	2-5	thin	Floor, centre	1.750	0.000	1.480
15	4	D	3-5	thin	Floor, high x	2.800	0.000	1.480
16	4	D	4-5	thin	Lab floor below house	1.470	-0.122	1.950
17	5	G	1-5	thick	Cold room, Wall, bottom	3.754	0.720	1.480
18	5	G	2-5	thick	Cold room, Wall, centre	3.764	1.700	1.480
19	5	G	3-5	thick	Cold room, Wall, top	3.764	2.670	1.480
20	5	G	4-5	thick	Cold room, Air	4.000	1.700	1.480
21	6	H	1-5	thick	Ext. wall Low X, bottom	-0.135	0.720	1.480
22	6	H	2-5	thick	Ext. wall Low X, centre	-0.135	1.700	1.480
23	6	H	3-5	thick	Ext. wall Low X, top	-0.135	2.670	1.480
24	6	H	4-5	thick	Ext. wall High Z, bottom	2.000	0.720	3.095
25	7	J	1-5	thick	Ext. wall High Z, centre	2.000	1.700	3.095
26	7	J	2-5	thick	Ext. wall High Z, top	2.000	2.670	3.095
27	7	J	3-5	thick	Ceiling, low x	0.690	3.439	1.480
28	7	J	4-5	thick	Ceiling, centre	1.750	3.439	1.480
29	8	K	1-5	thick	Ceiling, high x	2.800	3.439	1.480
30	8	K	2-5	thick	Lab air, bottom		0.720	
31	8	K	3-5	thick	Lab air, centre		1.700	
32	8	K	4-5	thick	Lab air, top		2.670	

* Coordinates from existing (before installation of EPS) internal wall surfaces, x from wall with inlet, y from floor, z from wall opposite door

ISSN 1901-726X
DCE Technical Report No. 053